Chemical Engineering Journal 440 (2022) 135739

Contents lists available at ScienceDirect

Chemical Engineering Journal

journal homepage: www.elsevier.com/locate/cej

Neutral inhibitor molecules entrapped into polypyrrole network for corrosion protection

Yue Yin, Manoj Prabhakar, Petra Ebbinghaus, Cauê Corrêa da Silva, Michael Rohwerder *

Max-Planck-Institut für Eisenforschung GmbH, 40237 Düsseldorf, Germany

ARTICLE INFO

Keywords:
Polypyrrole
Passivation
Scanning Kelvin Probe
Corrosion inhibitor
Inhibitor formulations
Anodic potential
Smart coating

ABSTRACT

For the performance of smart self-healing coatings, several factors are of critical importance: the type of inhibitors that can be released, the kind of trigger signal, the rate of trigger signal spreading and the transport capability in the coating for providing sufficiently fast sufficient amounts of active agents to the defect. In recent works, it was shown that intrinsically conducting polymer (ICP) applied between the metal and the top coating cannot only significantly enhance the signal spreading, but also the transport of active agents towards the defect. Hence, in combination nano-containers with ICP layers can play a crucial role in designing intelligent self-healing coatings. However, an interesting question is whether such ICP layers could also play a direct role in storing active agents and their smart release. Here, the idea is presented of entrapping inhibitor directly inside the ICP matrix. For this polypyrrole (PPy) coatings were electrodeposited in the presence of additions of β-Cyclodextrine, benzotriazole or 8-Hydroxyquinoline in the deposition electrolyte containing pyrrole and 3-nitrosalicylate (as counter-anion). The structure, composition, and morphology of these PPy coatings were evaluated by FTIR, Raman, XPS and SEM and the entrapment of the molecules was confirmed by triggered release and detection by UV–vis. The self-healing performance was investigated by monitoring both the corrosion potential in an electrolyte filled defect and the delamination behavior by SKP. An excellent performance in terms of an extraordinarily significant passivation effect is observed, which is proposed to be a consequence of a synergy between the inhibitors and re-oxidation of the PPy. Most notably, the delaminated interface is fully restored.

1. Introduction

Corrosion as a natural phenomenon occurs everywhere and causes enormous economic losses all over the world [1,2]. So, understanding the mechanism of corrosion and reducing the cost of corrosion by protecting against it is of great economic importance and often also enhancing safety against dangers caused by corrosion induced failure. In the past, chromate as a most efficient corrosion inhibitor, usually either added as chromate pigment to organic coating or applied as a chromate pre-treatment directly onto the metal, was widely used in many industries due to the excellent inhibition of corrosion and the resulting high efficiency of corrosion protection [3–5]. As the environmental standards are continuously improved, chromate as a hazardous corrosion inhibitor that endangers the public health and poses a serious ecologic problem has been banned in many countries. Hence, research for new highly efficient inhibitors is very important in corrosion science, just as well research in novel coating concepts that provide more efficient inhibitor supply to corrosion sites.

The use of intrinsically conducting polymers (ICPs) for new promising coating concepts has been widely investigated in the recent two decades [6–15]. In contrast to non-conducting organic coating, ICPs have an inherent redox activity which can e.g. re-passivate small pinholes in organic coatings [15,16]. More importantly, the redox-activity can be used to achieve a triggered release of the counter-anion stored in the ICP matrix to compensate the positive charge sitting on the polymer backbone of the ICP [13,14,17–36], and hence ICPs have been at the center of some of the earliest works on smart self-healing coatings [13,14]. However, it was shown by Michalik et al. [17] that for continuous layers of ICP or even too extended agglomerates of ICP no release of the counter-ions occurs, if a non-conducting top coating is applied on the ICP coating and/or the sample is not fully immersed into the electrolyte, with just the defect being covered by corrosive electrolyte (as e.g. in atmospheric corrosion, see also [17–19]). This is because then they become quickly cation permselective upon onset of reduction,

* Corresponding author.
E-mail address: rohwerder@mpie.de (M. Rohwerder).

https://doi.org/10.1016/j.cej.2022.135739
Received 12 November 2021; Received in revised form 18 January 2022; Accepted 9 March 2022
Available online 11 March 2022

which is in agreement with some claims that reduced ICP inhibits chloride diffusion [9]. For these cases triggered release from ICP is only possible when it is added e.g. as small nano-particles to a non-conductive coating matrix [9,14,17]. However, it was recently shown that continuous layers of ICP applied between metal and the non-conducting polymer matrix can not only significantly enhance the signal spreading for corrosion triggered release of active agents from suitable nano-containers [20], but also the transport of the released active agents towards the defect [21]. It would be highly desirable for achieving an even improved performance that the ICP layer could also directly participate in storage and triggered release of active agents. Hence, the idea of this work was to investigate whether neutral inhibitor molecules can be entrapped during deposition of ICP layers and whether they might then be released upon reduction of the ICP as a consequence of corrosion at a defect. Since ICP reduction usually increases the hydrophilicity of the ICP, this might enable the release of these molecules. It was decided to use electrochemical deposition of the ICP onto the metal surface, since this preparation avoids issues with the formation of an insulating interface between ICP and the metal, which often requires the use of spacer particles preventing direct contact between ICP and metal [22–24]. Namely, it was decided to electrodeposit PPy coatings onto zinc for these studies, as polypyrrole was found in our earlier works [20,21] to be a very suitable ICP and zinc is very relevant due to the fact that steel for advanced applications is nowadays usually galvanized.

As mentioned numerous works were done to study the release of counter-anions (anionic corrosion inhibitor) and the resulting effect on the corrosion performance. All these experiments were done under immersion conditions. Examples are electrodeposited PPy coatings on different non-noble metals, prepared by anodic oxidation of the monomer in the presence of supporting electrolyte with anionic inorganic corrosion inhibitors such as MoO_4^{2-}, $PMo_{12}O_{40}^{3-}$, PO_4^{3-} and WO_4^{2-} [29–36]. For instance, Ohtsuka et al. [29,30] prepared a bi-layered PPy coating consisting of an inner PPy-PMo_{12} (from $H_3PMo_{12}O_{40}$) and an outer PPy-NDS (from1,5-naphthalenedisulfonic acid disodium salt) layer to investigate the corrosion prevention of steel. The results showed that this coating system prevented corrosion of steel for a quite long time period, where the inner layer serves to passivate active steel sites and in the outer layer the large organic ions of NDS were proposed to restrict the decomposition of PMo_{12} ions in the inner layer. This system was shown to be capable of defect passivation. However, it has to be pointed out that this was an immersion experiment without an applied top-coating. Plieth and co-worker [19] reported of a PPy(MoO_4) coating with molybdate as counter-anion prepared on mild steel and observed a quite good corrosion resistance. Once the aggressive ions reached the mild steel most likely at pin-holes in the PPy, molybdate was released from the coating, stopping corrosion within the pinholes, in agreement with [15]. In another work, a PPy coating was prepared on carbon steel using oxalic acid solutions containing pyrrole and also additions of Na_2WO_4. The obtained results showed that this PPy coating showed good adhesion quite good protection of the carbon steel against corrosion in aggressive chloride containing electrolytes [33,34]. In all these cases, the protective property of the coating is determined by the capability to release the anionic counterions from the PPy coating. As mentioned, this release of counter-anions will be very limited with a top coating and/or for the case of atmospheric corrosion conditions and hence will work only for small defects such as pinholes.

Here, a new concept is proposed where neutral inhibitor molecules are entrapped in the ICPs coating, thus utilizing a new way for the storage of corrosion inhibitor into the ICP coating. To the best of our knowledge, entrapment of neutral inhibitor molecules during electrodeposition of PPy and its possible beneficial effect in its corrosion protection performance have not been investigated yet.

Although, BTA, β-CD and 8-HQ have been studied as corrosion inhibitors in chloride solutions for many years [37–41], until now only very little has been reported about the use of these corrosion inhibitors incorporated into ICP coatings. Montemor et al. [42] prepared PPy on AA6061-T6 in H_2SO_4 solution containing pyrrole in the presence of 8-HQ. They found that the compactness of the resulting PPy coating doped with 8-HQ can effectively mitigate the pitting corrosion of AA6061-T6 in chloride media and proposed that this may be due to a decrease of the migration of chloride ion into the coating. They did not report how 8-HQ might be incorporated and whether 8-HQ was released from the reduced PPy coating which might inhibit active corrosion sites. Breslin et al. [41] reported about electropolymerization preparing PPy-SβCD coating on a Pt electrode in pyrrole and anionic sulfonated β-cyclodextrin solution. This coating was then used as an electrochemical sensor for the detection of dopamine. Although, in that work the β-cyclodextrin was sulfonated and thus incorporated as an anionic counterion, it seems attractive to try to entrap neutral β-cyclodextrin in to the PPy coating for corrosion protection. It has been reported that β-cyclodextrin is a good inhibitor for corrosion protection of zinc [40]. A PPy coating containing BTA was formed on Cu through electrodeposition of pyrrole in oxalic acid (providing oxalate counterions) electrolyte containing BTA by Ohtsuka [43]. They emphasized the function of the ionized BTA to effectively form a BTA-Cu complex layer on the surface of Cu thus inhibiting the initial dissolution of copper and promoting adhesion of the PPy film on the copper. The coating was found to provide self-healing of an artificial defect during immersion in 3.5% NaCl aqueous solution. The quite good corrosion protection behavior was suggested to be caused by synergistic effects of the oxidative property of the PPy film and the inhibitive property of oxalate and the adhesion promotion of the BTA. This work focusses on the BTA adsorption onto the copper surface to improve the corrosion resistance, not possible BTA entrapment into the PPy coating. Dong [44] et al. prepared PPy on Cu together with BTA or/and silica in salicylate solution and found that the presence of only BTA or only silica in the PPy film improved the corrosion resistance only slightly, but in combination a significant improvement was found. They suggest that this good performance was attributed to the synergetic effect from the physical barrier of silica and the active protection by the BTA. However, they did not provide a direct proof of BTA release from the PPy coating.

In all the above-mentioned papers, inhibitor incorporation as counterion was assumed and not the possibility of entrapment as neutral inhibitor molecules into the PPy network. Furthermore, as mentioned in all these cases no long-range transport of the inhibitor was required (or investigated), i.e. these studies were performed under conditions, where also sufficient release of an inhibitor incorporated as counter-anion is still working, i.e. under immersion of the whole sample in electrolyte, without top coat and usually in the presence only of small defects or pinholes. The situation is different when a non-conductive topcoat is applied on the ICP and there is a larger defect, and especially also when the condition is rather one of atmospheric corrosion where electrolyte is rather only on the defect, but not on the whole coating, see e.g. [18]. Then release and transport have to occur over a certain distance from the defect. As mentioned above, under such condition the PPy becomes quickly cation permselective and only limited anion release would be observed. Instead cation incorporation occurs for ensuring charge neutrality upon reduction of the ICP [17].

Here, the key question now is, whether under such condition release of entrapped inhibitor might occur and whether it might work well even across longer distances in the ICP. Furthermore, in most of the above discussed works the release of the corrosion inhibitor from the ICPs coating is just assumed (and it is often unclear whether the observed effect is mainly due to the released counter-anion or possibly entrapped molecules). No experiments were carried out to investigate this in more detail by chemical analysis. In addition, usually it is unknown whether corrosion inhibitors which are added to the deposition bath in addition to the anionic inhibitor which will be incorporated as counter-anion may really be also incorporated into the ICP matrix. As discussed, often they are considered just to improve the interfacial adhesion between substrate and ICP.

In order to elucidate the potential of entrapped inhibitor molecules

for smart corrosion protection, based on our previous study, where we investigated the transport of different inhibitors through the (partially reduced) PPy matrix [21], we designed a dedicated study for investigating the entrapment of neutral inhibitor molecules (BTA, β-CD, 8-HQ) into the PPy matrix, their release and their effect on corrosion inhibition of a defect under atmospheric corrosion conditions. In these investigations the PPy coating was always covered by a non-conducting PVB coating. Hence, transport of the inhibitor had to occur through the PPy to the defect.

For achieving entrapment of neutral (or at least non-anionic) inhibitor molecules, the electrodeposition of PPy was carried out in the presence of 8-HQ, BTA or β-CD. As counter-anion to be incorporated for charge-compensation 3-nitrosalicylic acid (3-Nisa) was chosen, because we have considerable experience with electrodeposition of PPy(3-Nisa) on zinc, as well as with the required pretreatment of the zinc prior to the electrodeposition [20,21]. The reduction and delamination of the PPy/PVB coating system was monitored by SKP, as well as the evolution of the corrosion potential in the defect. The idea was to investigate in how far also for entrapped inhibitor smart corrosion-triggered release could passivate the defect and even lead to a self-healing of the delaminated interface. As in accordance with our earlier findings [17,20,21] release of the 3-Nisa is negligible under these conditions of using a continuous PPy layer, successful inhibition of corrosion and self-healing would be a clear indication for release of the entrapped inhibitor molecules 8-HQ, BTA or β-CD. In a previous work, it was already shown that these inhibitors are highly mobile in partially reduced PPy [21]. It will be shown in this work that thus a new smart coating system can be designed that is not only capable of inhibiting corrosion in the defect but also to restore the delaminated metal/coating interface.

2. Experimental procedure

2.1. Electrochemical deposition of the PPy coatings

Pyrrole monomer (Aldrich) was distilled twice under inert atmosphere. 3-Nitrosalicylic acid (3-Nisa, purity 99%), β-Cyclodextrine (β-CD, purity 97%), potassium chloride, potassium hydroxide, sodium hydroxide, ethanol, tetraethylammonium-p-toluenesulfonate ($N(Et)_4Tos$, also called tetraethylammonium tosylate), tetrabutylammonium chloride, benzotriazole (BTA), 8-Hydroxyquinoline (8-HQ, purity 99%) and poly(vinyl butyral-co-vinyl alcohol-co-vinyl acetate) (PVB) (MW≈50000-80000 g/mol) were purchased from Sigma-Aldrich and used as received. All other reagents were analytical grade and purchased from Sigma-Aldrich. Ultrapure water was obtained from a Millipore-Milli-Q System with a resistivity near to 18.2 MΩ·cm.

The solution used for the electrodeposition of the PPy layers was prepared as follows: 0.01 M 3-Nisa were dissolved in de-ionized water and then 0.3 M pyrrole were added into the solution. For preparing PPy coatings with entrapped inhibitor in addition to the 3-Nisa that is incorporated as counter-anion, either 0.01 M β-CD, 0.003 M 8-HQ, or 0.1 (or 0.001 M) M BTA was added into this solution. Then the pH of the solution was adjusted to 2.5 using KOH. The resulting samples were denoted as PPy-β-CD, PPy-8-HQ and PPy-BTA, depending on the neutral inhibitor molecule that was tried to be entrapped. The Zn (20 mm × 10 mm × 1.5 mm) samples were mechanically ground with SiC papers of various grit size ranging from P400 to P2500. After grinding, the substrates were washed using distilled water and then rinsed with ethanol to remove contaminations and dried in N_2. Furthermore, a pretreatment of the zinc surface was carried out prior to electrodeposition of the PPy in a three-electrode cell under potentiodynamic regime by sweeping the potential for 5 cycles between −1.1 V to −1.4 V vs $Ag/AgCl_{(3\ M\ KCl)}$ in 0.25 M NaOH [20,21] at a scan rate of 10 mV/s using a Voltalab 50 potentiostat. A $Ag/AgCl_{(3\ M\ KCl)}$ electrode and a platinum foil were used as reference and counter electrodes, respectively. This resulted in a ZnO layer with a thickness of about 30 nm layer, which was found to effectively inhibit the dissolution of Zn during the following electropolymerization process [21]. After pretreating, the electrodeposition of PPy was realized galvanostatically at a current density of 3 or 5 mA/cm^2. The total charge passed for the formation of the coating was 1.25 C/cm^2. An area of 8 mm × 18 mm was exposed to the stirred aqueous electrolyte solution (~40 mL). The samples were rinsed immediately after electrodeposition with H_2O and EtOH and dried in a N_2 stream. The PPy(3 mA/cm^2) and PPy-BTA were formed at a constant current of 3 mA/cm^2 for 417 s. The PPy(5 mA/cm^2), PPy-β-CD and PPy-8-HQ were formed at a constant current of 5 mA/cm^2 for 250 s.

In order to study the leaching and release of entrapped inhibitor from the PPy, dedicated experiments were performed with the PPy-BTA coating. For this, a layer of PPy-BTA was electrodeposited on a glass sample coated with an ultra-thin evaporated of Au, in 0.1 M $N(Et)_4Tos$ + 0.3 M pyrrole + 0.1 M BTA solution with current density of 2 mA/cm^2 for 200 s. The reason for using tosylate as counter-anion instead of 3-Nisa counter-anions is that the UV–vis adsorption peaks of 3-Nisa and BTA overlap. Since on gold no 3-Nisa as inhibitor to passivate the surface is required, tosylate could be used in this case, thus reducing the problem of overlapping peaks (some overlap remains).

For the investigation of cathodic delamination and self-healing performance of the different PPy coatings, an additional PVB-topcoat was applied onto the PPy coatings in order to ensure that release and transport of inhibitor had to occur laterally through the coating, i.e. to prevent release vertically into electrolyte. Such an additional non-conductive topcoat is very relevant, as this will be the case also in most technical applications. For this, samples were spin-coated 4 times with a 5 wt% PVB solution at 2000 rpm for 20 s, and then spin-coated 3 times with a 10 wt% PVB solution at 2000 rpm for 20 s, respectively. After both processes the samples were dried in an oven at 75 °C for approx. 10 mins.

For comparison, also experiments were performed without PPy where the three inhibitors β-CD, 8-HQ and BTA were added directly into PVB. For this 0.01 M β-CD, 0.003 M 8-HQ, or 0.1 M BTA were mixed with 5 wt% PVB, which then was coated on Zn substrate by spin-coating 4 times, and then spin-coating 3 times with a 10 wt% PVB solution as topcoat, respectively. These sample are denoted in the following as PVB-β-CD, PVB-8-HQ and PVB-BTA.

2.2. Measurement and characterization

The different PPy coatings without topcoat (PVB) were characterized by FTIR, XPS, Raman and SEM. The morphology of the coatings was investigated by scanning electron microscopy (SEM; LEO 1550VP, Carl Zeiss). Fourier transform-infrared (FTIR, a Bruker Vertex 70v Fourier transform IR spectrometer) spectroscopy was used to measure the PPy coating with and without entrapped corrosion inhibitor. FTIR spectra were also obtained of pure β-CD, 8-HQ, or BTA. The test specimens for this were prepared by the KBr-disk method. FTIR was also used for characterization of the PVB composite coatings containing neutral inhibitor molecules. The functional groups present in these samples were analyzed by FTIR in the wavelengths range from 400 to 4000 cm^{-1}. Raman measurements of the coatings were performed using a Labram confocal Raman microscope (Horiba Jobin Yvon, France), equipped with an Ar laser source (emission wave-length: 514.5 nm). The laser power for the excitation was maintained below 5 mW to avoid sample destruction. X-ray photoelectron spectroscopy (XPS) was performed using a monochromatic Al Kα1 source (1486.7 eV) operated at 15 kV and 25 W from PHI (Quantera II), a pass energy of 29.35 eV and a step size of 0.125 eV was used to obtain high resolution spectra. The XPS data were all processed and analyzed with CASA XPS.

Measuring the rate of benzotriazole leaching. UV–vis spectroscopy (Perkin Elmer Lambda 800) was used to assess the leachable amount of BTA from the PPy($N(Et)_4Tos$)-BTA coating in 1 M KCl or 0.05 M tetrabutylammonium chloride.

Global release (fully immersed sample, without top coat): In a typical release experiment PPy($N(Et)_4Tos$) with entrapped BTA was

immersed in 20 mL buffer solution. Experiments on leaching of the immersed samples and also on electrochemically triggered release of BTA and tosylate by reduction of the PPy coating were carried out, the latter by use of the above mentioned three electrode set-ups. To investigate the potential triggered leaching of BTA and tosylate, the coating was reduced at −500 mV_{SHE}. Aliquots of 0.5 mL were taken from the solution, followed by the addition of 0.5 mL fresh buffer solution at different time intervals for 10 h.

Release from the edge: In order to further simulate the more relevant lateral long-distance release of BTA from the PPy($N(Et)_4Tos$) with entrapped BTA with a top coat, a setup was designed as shown in Fig. 1. For the immersion experiment, the BTA and tosylate were released by plain diffusion from the intact (not reduced) coating to the defect. To investigate potential triggered release the BTA and tosylate release, the coating was reduced at −500 mV_{SHE}. After 10 h diffusion and transport, the solution in the defect site was collected to measure the BTA and tosylate.

Scanning Kelvin Probe (SKP) was used to evaluate the cathodic delamination of the coating and the self-healing performance at the defect. The defect was made by a razor blade with a size of 2.6 mm ± 0.2 mm long, 58 µm ± 6 µm wide, and 34 µm ± 4 µm deep. The defect was filled with 1 M KCl solution and then introduced into the SKP chamber with a relative humidity of 93%. The SKP tip was directly placed over the KCl solution at the defect, with a volume of 7.5 µL, in order to monitor the electrode potential. Cathodic delamination was monitored by line scans over 3 mm with a step size of 10 µm. Before the experiment, the SKP tip was calibrated against a $Cu/CuSO_4$ (saturated) reference electrode [45].

3. Results and discussion

3.1. The morphology of the PPy coatings

The morphologies of the PPy coatings on the Zn substrate with and without entrapped corrosion inhibitors in addition to the 3-Nisa incorporated as counter-anion are shown in Fig. 2. There is no marked morphological change caused by the different current densities in Fig. 2 (a) and (c) for the PPy coatings galvanostatically deposited at 3 or 5 mA/cm^2. In both cases the morphology was found to consist of a uniform globular structure associated with some degree of microscopic ruggedness. The quality of the coatings was obviously quite good as no cracks or detachments of the coating were observed. The PPy coatings exhibit a homogeneous, compact cauliflower-like appearance, in which small spherical grains with a few micrometer diameters conglomerated. The cauliflower structure is proposed to be due to the difficulty of counterion incorporation in the polymeric chain [46]. This type of structure was observed in the case that counterions were not able to easily intercalate into the polymer chain and is assumed to be correlated to a relatively low concentration of counter-anions.

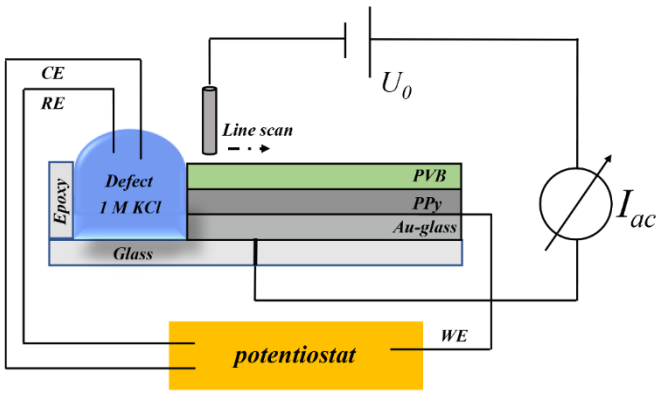

Fig. 1. The setup for the edge release BTA and tosylate from the PPy($N(Et)_4Tos$)-BTA coating.

Concerning the coatings with entrapped corrosion inhibitor, the morphologies of the PPy(5 mA/cm^2) and PPy-β-CD are very similar, for both a similar typical cauliflower-like morphology is observed. However, it can be clearly seen that the corrosion inhibitors 8-HQ and BTA have a strong effect on the morphologies of the resulting PPy coatings. For the PPy-BTA coating (prepared at 3 mA/ cm^2), the surface is more uneven than PPy(3 mA/cm^2), and there are many small particles on the surface. The figure inserted in Fig. 2 (b) shows that there are severe agglomerations leading to quite big particles. The globular structures range between 0.5 µm and 12 µm (see Fig. 2 (b)). Concerning the PPy-8-HQ coating, there are many tiny particles on the surface and it looks more homogenous. The inserted figure shows that the surface of the particles is smooth and no small particles adhere on the surface of the big particles. So, for the case of BTA and 8-HQ the entrapped corrosion inhibitor will change the growth of the coating, and cause a morphology change.

3.2. Structural characterization of the PPy coatings

In Fig. 3 the FTIR spectra of PPy coatings with or without entrapped additional corrosion inhibitors are shown. The characteristic PPy absorption peaks exhibit the same features as for standard PPy films, which were previously reported [31,36,41,47–51]. Except for the peak around 3400 cm^{-1}, no spectroscopic differences between films prepared at 3 mA/cm^2 and those prepared at 5 mA/cm^2 were formed. This very large absorption band located in the spectral domain around 3400 cm^{-1} is characteristic of –OH functional group belonging to residual water molecules trapped in the PPy matrix. A strong band at 2930 cm^{-1} is attributed to the C–H stretching vibration. The weak band around 1500 cm^{-1} is due to C = C stretching vibration. The band at 1436 cm^{-1} is ascribed to the breathing and the stretching vibration of C–C in the pyrrole ring. The band at 1244 cm^{-1} in the spectra of PPy coating is attributed to the in-plane deformation of the C–N bonds in the pyrrole units. Bands at 754 and 951 cm^{-1} are assigned to the out-of-plane vibration of the C–H bonds of the aromatic rings. The weak peak around 881 cm^{-1} is assigned to C–H in plane stretching vibration. The wide and strong adsorption bands situated at 1550–1750 cm^{-1} are attributed to the C = C stretching, C–N in-plane bending vibrations of pyrrole ring and C = O stretching vibration. The weak band at 1073 cm^{-1} corresponds to the in-plane deformation of the N–H bonds. The weak band around 1121 cm^{-1} is due to C–C stretching vibration of pyrrole nucleus. The presence of the C = O band might indicate some degree of overoxidation of the PPy during the electrodeposition, but most likely is at least partially -if not fully- corresponding to the C = O group in 3-Nisa, which is the counter-anion in all these coatings. However, all these spectra are very similar regardless of the entrapped inhibitor, they all revealed the typical PPy structure. Hence, no IR sensitive changes of the PPy structure caused by the entrapment of the neutral inhibitor molecule can be identified here.

FTIR analysis was also used to study the possible interaction between corrosion inhibitor and organic matrix of the non-conducting PVB. The FTIR spectra in Fig. 4 were obtained for the pigmented and unpigmented PVB coating, in which the corrosion inhibitor was just physical mixed into the PVB. The FTIR spectrum of PVB-BTA (Fig. 4 (a)) shows two main bands at 746 and 775 cm^{-1}, which are attributed to C–H out of plane vibrations of the hydrocarbon in the benzene ring. The peak at 1005 cm^{-1} indicates the stretching vibration of N–C on the benzene ring. The two bands at 1049 and 1141 cm^{-1} are assigned to the triazole stretching vibrations with a small contribution of C–H bending. The strong peak at 1210 cm^{-1} represents the triazole stretching vibration of N = N from the BTA [52–54]. Overall these peaks indicate that BTA molecules are present in the PVB coating and the spectra show no indications that BTA mighty undergo a reaction with PVB.

The spectra of 8-HQ and PVB-8-HQ are shown in Fig. 4 (b). The vibration modes of benzene rings are at 1575, 1503, 1164, 1059, 815, 779

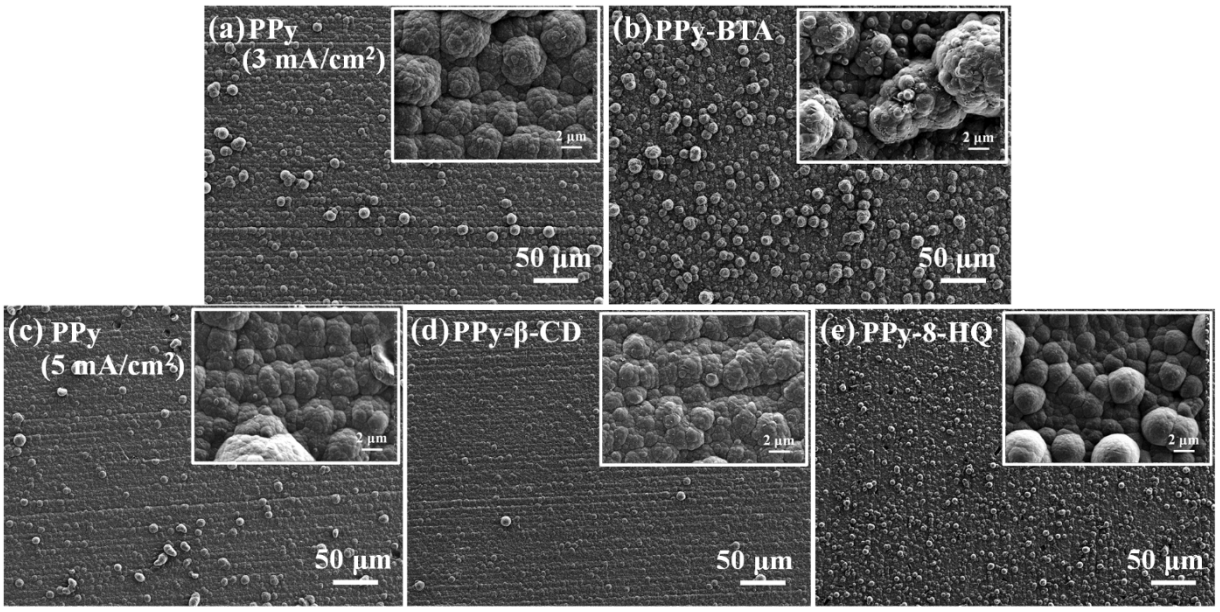

Fig. 2. The surface morphology of PPy coatings on Zn substrate doped with the different corrosion inhibitors.

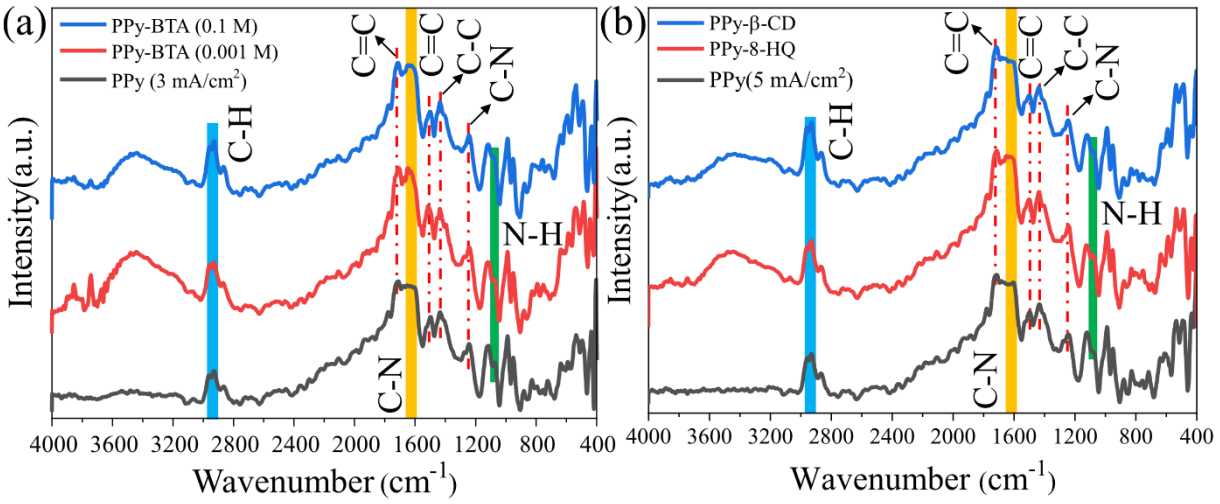

Fig. 3. The FTIR spectra of PPy coatings on Zn substrate without or with the different entrapped corrosion inhibitors.

and 491 cm^{-1}. The peak at 1575 cm^{-1} is attributed to the C–C group. The bands at around 1503 and 1470 cm^{-1} are associated with the stretching vibration of aromatic C–C and C–N in the 8-HQ structure. The vibration mode of C = N is at 1377 cm^{-1}, the bending vibration mode of C–N is at 1279 cm^{-1}, and the stretch vibration modes of C–O are at 1223 and 1203, 1093 cm^{-1}. The bands at 573 and 465 cm^{-1} correspond to in-plane and out-of-plane bending of C–O, respectively. The peak at 1377 cm^{-1} represent C = N shows that the 8-HQ is present in the PVB without reacting with it [55,56].

The FTIR spectra of β-CD and PVB-β-CD are shown in Fig. 4 (c). The band at 1648 cm^{-1} is attributed to O–H bending. The peaks at 1158 and 1028 cm^{-1} are assigned to the asymmetric C–O and the symmetric C–O–C stretching vibration, respectively. In the region 1400–1200 cm^{-1} are the absorption bands of the deformation vibrations of the C–H bonds of β-CD (1369, 1337 and 1254 cm^{-1}). The absorption bands in the region 950–700 cm^{-1} belong to the deformation vibrations of the C–H bonds (942, 858, 758 and 707 cm^{-1}) and the pulsation vibrations in the glucopyranose cycle [57,58]. The FTIR spectrum of the PVB-β-CD is similar to that of β-CD, indicating that the frame of β-CD in the complex is not changed and β-CD can stable exist in the PVB coating.

Raman spectroscopy was also used to obtain more information on the structure of the PPy coating compared to PPy coating containing entrapped inhibitor. The Raman spectra of PPy coating on Zn substrate shows the principal bands of PPy, which are in accordance with what is reported in the literature [36,59–61]. PPy coatings electrodeposited on Zn with or without corrosion inhibitors generally have the same structural features, as can be seen in Fig. 5. A highest intensity peak around 1580 cm^{-1} characterizes the stretching of the conjugative backbone C–C = C ring. The obtained peak at 1368 cm^{-1} is associated to the anti-symmetrical C–N stretching of PPy. The peak at 1307 cm^{-1} is assigned to antisymmetric C–H deformation vibrations. The peak at 1238 cm^{-1} corresponds to the C–C stretching and the anti-symmetrical C–H in-plane deformation. The peak related to the N–H in-plane bending and the symmetrical C–H in-plane deformation is found at 1041 cm^{-1}. The representative peak at 957 cm^{-1} is attributed to the ring deformation vibrations indication units and radical cation. The peaks at 922 and 1084 cm^{-1} are attributed to the ring deformation and the symmetrical C–H in plane bending.

Consequently, Raman and Infrared spectra confirm that the corrosion inhibitor entrapment into the PPy coating did not cause a change of

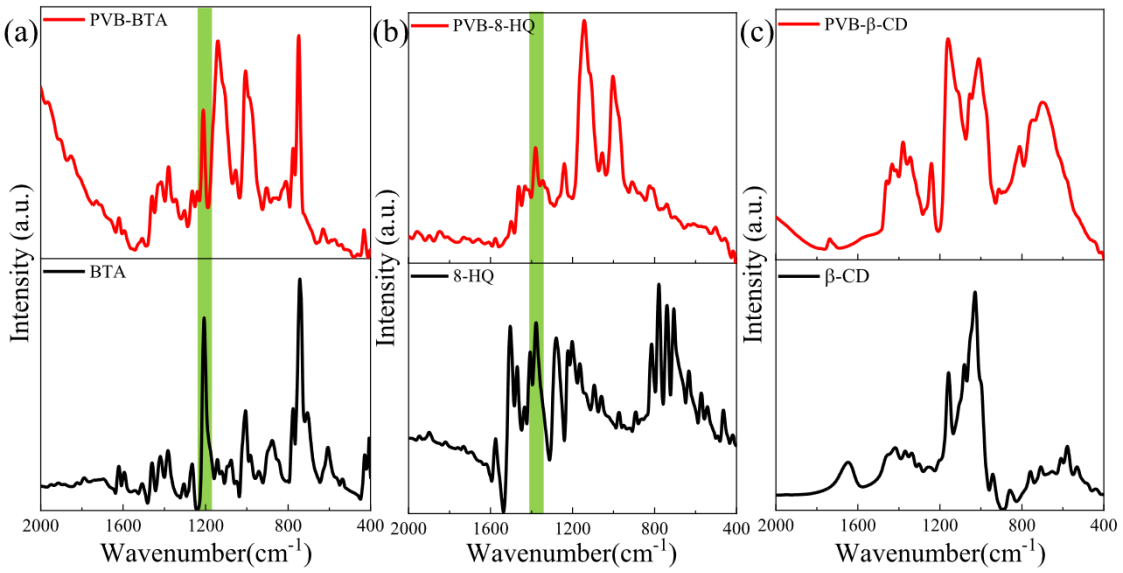

Fig. 4. FTIR spectrum of coating with inhibitor mixed with 5 wt% PVB coated on Zn (a) PVB-BTA, (b) PVB-8-HQ, (c) PVB-β-CD.

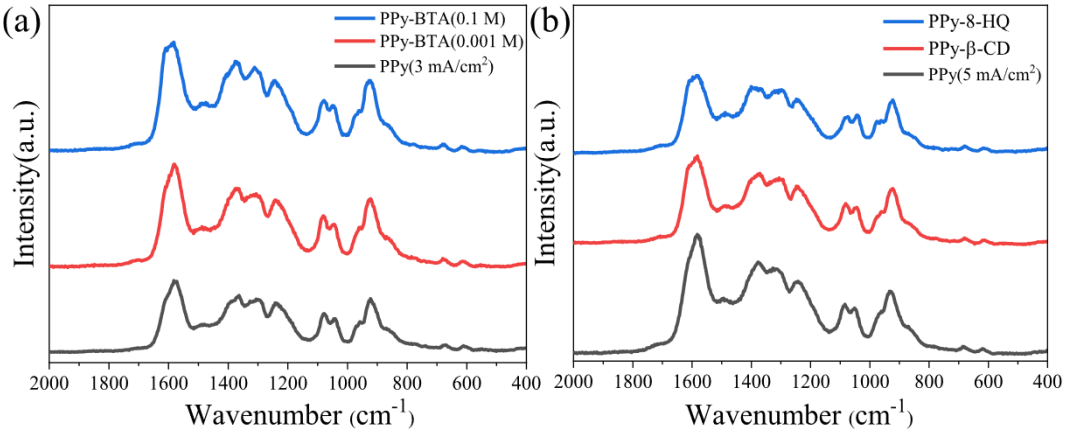

Fig. 5. The Raman spectra of PPy coatings on Zn substrate with or without different entrapped corrosion inhibitors.

the structure of PPy coating. The Raman spectra do not provide proof for the presence of corrosion inhibitors in the PPy coating. This is due to the similarity of the functional groups of the corrosion inhibitors with the functional groups of the counterions and the pyrrole. However, the IR spectra shown in Fig. 4 at least provide at least sound indications for the presence of the different inhibitors.

Also, XPS was applied for a characterization of the PPy with and without entrapped inhibitor. Fig. 6 (a) shows the deconvoluted high resolution N 1 s spectrum of the PPy with or without entrapped inhibitor. The entrapped corrosion inhibitors seem to have no effect on the state of N 1 s in the PPy coating. For the PPy(5 mA/cm^2) and PPy(3 mA/cm^2) coatings the peak consists of three peaks around 398.6 eV, 399.8 eV and 400.5 eV. For PPy-8-HQ, PPy-BTA and PPy-β-CD coating, an asymmetric peak centering at 399.6 eV is attributed to the neutral amine-like nitrogen (–NH–) at the pyrrole ring for the unoxidised N atom. The lower binding energy peak at 398.3 eV is assignment to imine-like nitrogen, –C = N. The peak at 400.9 eV is attributed to the positively charged nitrogen (–NH$^+$–, =NH$^+$–) due to the oxidized N atom [62]. This positively charged nitrogen, known as polarons for –NH$^+$– and bipolarons for = NH$^+$–, is an important parameter to indicate the oxidation degree of nitrogen in PPy coating. For the PPy-BTA coating, this peak is divided into two peaks at 400.9 and 400.2 eV.

Fig. 6 (b) shows the deconvoluted high resolution C 1 s spectrum for the PPy coating with and without entrapped corrosion inhibitors. The high-resolution C 1 s spectra for PPy(5 mA/cm^2), PPy(3 mA/cm^2), PPy-8-HQ, PPy-BTA and PPy-β-CD have all a very similar appearance. The carbon signal of C 1 s was deconvoluted into three peaks around 284.7, 285.9 and 287.8 eV. The main peak at 284.7 eV corresponds to C–C/C–H groups of the pyrrole nucleus, the different corrosion inhibitors and the counterion. The peak at 285.9 eV was assigned to C–N groups in the pyrrole rings and C–OH groups of the counterions. The binding energy peak at 287.8 eV was ascribed to carbonyl O–C = O groups. The appearance of C = O groups was mainly due to the presence of pyrrole over-oxidation during polymerization in aqueous media or from the counterion (3-Nisa).

Fig. 6 (c) shows the high-resolution O 1 s spectrum, which can be divided into three peaks at 531.3, 532.4 and 533.1 eV. No marked differences are observed in the O 1 s region for PPy coatings obtained with different corrosion inhibitors. The presence of oxygen atoms is an evidence of the counter-anion (3-Nisa) in the PPy coating. The peak located around 531.3 eV is attributed to C = O groups. This peak is contributed mainly by the oxygen atoms of the carboxylic acid groups in the 3-Nisa and maybe also partial over-oxidation of PPy. The weak peaks at 533.1 eV and 532.4 eV are assigned to C–O groups, water and the hydroxyl group from the counterion [63–66].

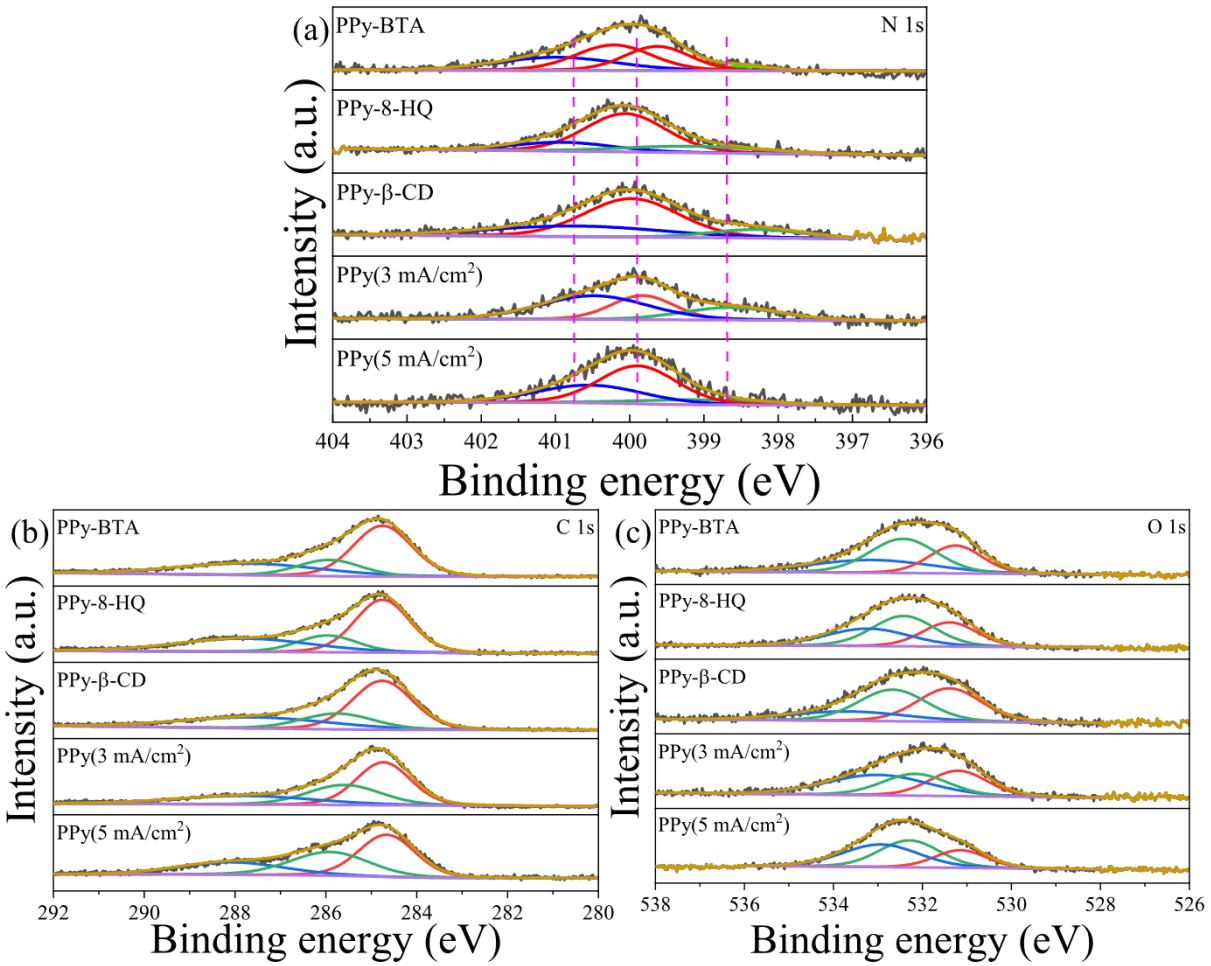

Fig. 6. XPS high resolution spectra for C 1 s, O 1 s and N 1 s of PPy coatings on Zn substrate with or without the different corrosion inhibitors.

3.3. The self-healing properties of neutral inhibitor molecules in coating matrix

3.3.1. Non-conducting organic matrix

Non-conducting organic coatings with additions of pigments or of inhibitor loaded nano-containers to the matrix are the standard in corrosion protection by organic coatings. Most of the related research just focusses on the active agent and the nano-containers to improve the corrosion resistance of the coating. However, the function of the organic coating matrix for enhanced transport of the active agent towards the corroding defect is a widely neglected factor. But actually, this property will play an important role for enhancing the self-healing performance of coatings [21]. Another point is the compatibility of the organic coating matrix and active agents. If the active agent reacts with the matrix, its mobility will be too low to reach the defect sufficiently fast and in sufficient amounts to passivate the defect and to restore the already disbonded area. In principle, a coating with a high resistance against delamination is an already quite good coating for corrosion protection. However, such a coating can only provide passive protection and will not provide protection to a corroding defect site. Actually, for designing high performant self-healing coating we propose in our earlier work that a fast delamination of the coating is a prerequisite condition for promoting fast active agent release and also its fast transport to the defect site [20,21]. For such concept to be successful, of course, self-healing of the interface has to occur simultaneously with the passivation of the defect or shortly after, thus re-establishing an intact coating. This requires an optimized combination of suitable active agents, their compatibility with the coating matrix, a suitable smart storage (e.g. in a switchable nano-container), fast trigger signal spreading for their release and fast transport to the defect. Here, the possibility of inhibitor entrapment in the PPy matrix as smart storage, the release of the inhibitor and its transport to the defect as well as its corrosion inhibition performance at the defect and the delaminated interface were studied.

As reference, also experiments were performed without PPy, where the inhibitors were just directly added to the PVB matrix. In Fig. 7 delamination profiles and the evolution of the corrosion potential in the defect are shown for these coatings with the three different inhibitors are shown, each with an additional PVB coating applied as topcoat. As can be seen, the type of the corrosion inhibitor has an influence on the potential of the intact coating. For the PVB-BTA, the potential of the intact coating is about −200 mV_{SHE} and thus about 200 mV higher than for the unpigmented sample [22,23]. The PVB-β-CD and PVB-8-HQ show potentials of the intact interface with zinc close to −400 mV_{SHE}, which is about what is obtained also for the unpigmented PVB on zinc [21,22]. For the samples PVB-β-CD and PVB-8-HQ, the corrosion potentials in the defect clearly indicate active corrosion of Zn (−700 to −800 mV_{SHE}). With increasing time, there is basically no change in the potential in the defect. That means that for both inhibitors no sufficient transport from the delaminated area to the defect to passivate the defect site occurs. Only the PVB-BTA sample shows an anodic shift of the potential around 200 mV in the more positive direction towards about −600 mV_{SHE} indicating a slight passivation of the defect.

For the PVB-BTA sample the delamination progress and the potential at the delaminated area show a distinctively different behaviour from the unpigmented PVB coating, and also from the other two pigmented coatings. As already mentioned, the intact interface has a higher

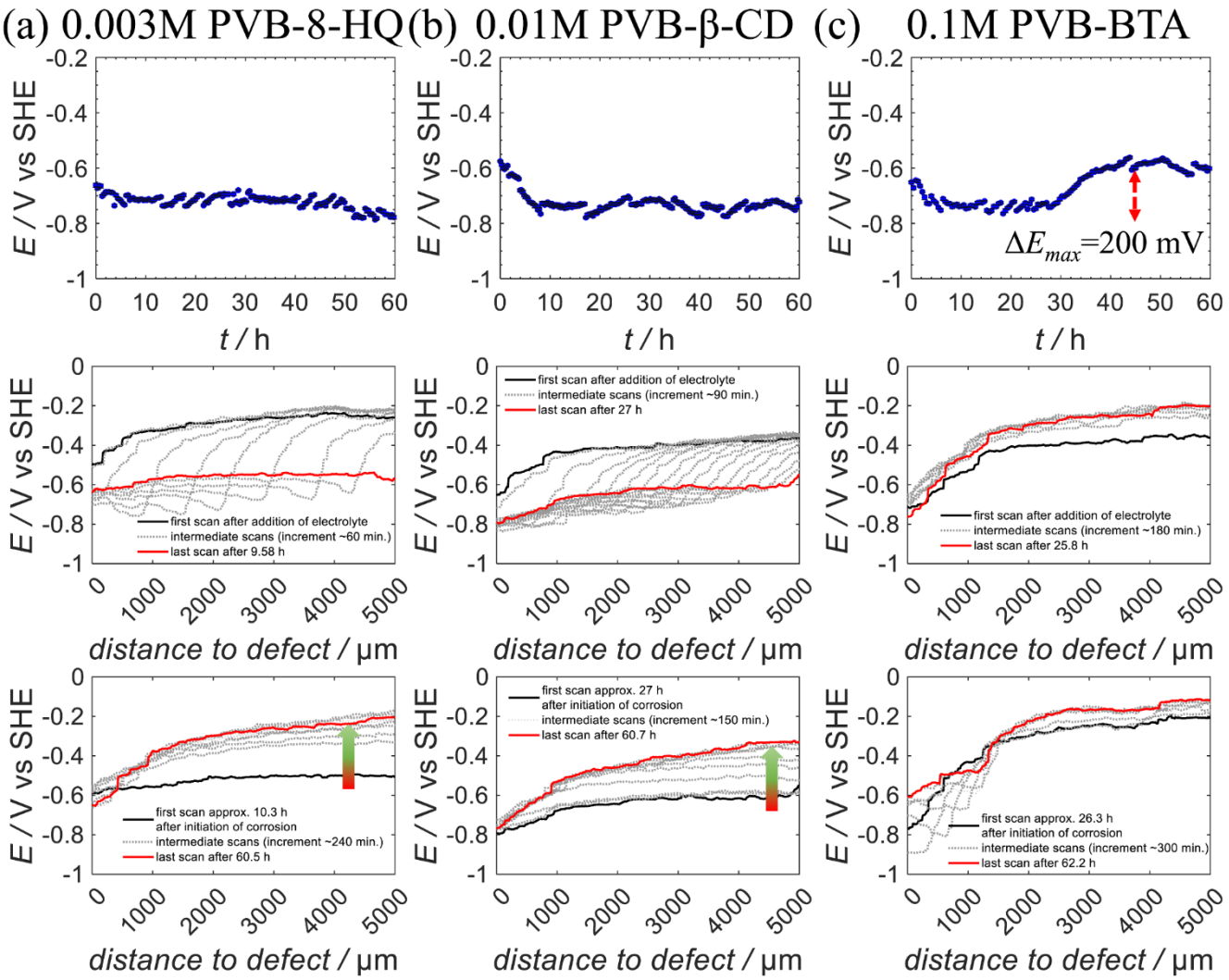

Fig. 7. Delamination profiles and electrode potential at the defect for PVB coatings containing the three different corrosion inhibitors applied on Zn substrate.

potential than the other coatings, moreover the delamination progress is slower than for the PVB-8-HQ or PVB-β-CD coatings and much slower than for just PVB [21,22]. With increasing time for all three coatings with entrapped inhibitor the potential within the delaminated zone increases. Further away from the defect even potentials of passive zinc of −400 mV_{SHE} are reached even when potentials of about −800 mV_{SHE} directly after delamination occurred, indicating that the interface was fully delaminated. However, only the coating with BTA shows potentials that are typical for passive zinc also at the initially delaminated interface close to the defect (−500 mV_{SHE}). These results show that for all three coatings passivation and re-establishment of a protective interface is achieved, blocking galvanic coupling to the defect site. For the PVB coatings with 8-HQ or β-CD this is, however, less effective than for the one with BTA. Furthermore, for the PVB-BTA sample, there is right away a quite significant inhibition of cathodic delamination. After 60 h, the BTA leached from the PVB shows a high efficiency to passivate the whole delaminated area and a protective interface is obviously restored. The relatively long time necessary for this indicates that the leaching of BTA from the PVB matrix is a slow process. Obviously, the accumulation of a sufficiently high concentration of BTA at the delaminated area and especially its transport to the defect site needs a certain period.

In principal, a faster delamination could activate more coating volume and provide an improved transport of leached inhibitor to the defect [20,21]. Since the cathodic delamination is significantly slowed down for the PVB with inhibitors, this certainly explains the failed or for the BTA quite delayed and limited passivation of the defect. Passivation of the delaminated interface does not, on the other hand, require long range transport. This indicates clearly the limitation of leaching from the PVB. Note also that the increase of potential at the delaminated interface does not only indicate passivation but also the restoring of a blocking interface, because for the potential to increase while the defect potential remains much lower, ionic mobility between defect and that interface has to be significantly blocked. Since a faster delamination is in principle beneficial for also faster leaching of corrosion inhibitor from the coating matrix, one would expect that the coatings containing β-CD or 8-HQ, which show a much higher initial high delamination rate than the coating containing BTA, should show a better defect passivation. But the results indicate that no or just a small amount of corrosion inhibitor reached the defect. However, the BTA containing coating shows the opposite. With a slower delamination rate than the samples with β-CD or 8-HQ, it shows a higher efficiency for leaching and supplying sufficient inhibitor to the defect. The corrosion inhibitor transport not only depends on the organic coating matrix, but also is determined by the structure of the corrosion inhibitor or rather by the interaction between these both. In how far the results indicate that there are differences in the mobility of the different inhibitors in the PVB cannot be concluded here for sure. It could also be that the much lower additions of β-CD or 8-HQ play a role here.

3.3.2. Conducting polymer matrix

In a next step it was further investigated whether ICP coatings can entrap cationic or neutral inhibitors into their matrix and whether that can be used for designing smart release coatings. For this it is first of all important to consider the charge of the different inhibitors in dependence on pH. For BTA as an amphoteric compound, the charge of BTA much depends on the pH [67,68]. When the pH is lower than 4, the BTA is protonated and hence carries a positive charge. For pH levels higher than 7, BTA is deprotonated with a negative charge. For pH values ranging from 4 to 7, there is no reliable information whether BTA exists in neutral or cationic forms. In our case, when we prepare the PPy-BTA coating, the pH of the electrolyte is pH 2.5. That means the BTA will be incorporated positively charged and cannot be incorporated as a counter-anion into the PPy coating. Instead it has to be entrapped otherwise. During exposure of the PPy to neutral electrolyte, it may finally be entrapped even in an uncharged state. Concerning β-CD and 8-HQ, according to literature β-CD does not deprotonate at pH < 12.0, that means the β-CD should be neutral in our experiment condition [69]. However, 8-HQ is reported to exist in the four prototropic species normal, tautomeric, cationic, and anionic species depending on the pH of the solution. At the pH of electrodeposition of the PPy coating in acid medium it should be neutral [70]. Hence, all three inhibitors will be entrapped inside the PPy matrix and not be incorporated as counter-anions.

Here, the three different inhibitors BTA, β-CD and 8-HQ were entrapped into the PPy matrix and the same studies described in the last section carried out for PVB as matrix were performed now for the case of PPy as matrix. Prior to studies on corrosion protection of the neutral inhibitor entrapped into the PPy coating, the corrosion driven cathodic delamination of PPy(3 mA/cm^2) and PPy(5 mA/cm^2) coatings from the zinc substrate was initially studied to obtain baseline kinetics. The results are shown in Fig. 8. The cathodic delamination process of PPy coatings from zinc has been studied in detail in prior works [20,21]. A uniform potential value range between 200 mV_{SHE} to 400 mV_{SHE} is observed for both cases for the intact coating, which is in agreement with PPy in its conductive and oxidized state. With the progress of delamination, the potential drops to a potential that is in accordance with freely corroding zinc, indicating reduction of the PPy and delamination. During the measurement, the PPy coating without entrapped inhibitor completely de-adhered within 3 h over the 3 mm that were scanned by SKP and the potential at the defect stayed at the one of free corrosion of Zn (−700 to −800 mV_{SHE}) for the whole duration of the measurement, i.e. 15 h. That means that no or just a low amount of 3-Nisa was released during the reduction of PPy, not enough to passivate the defect. This is in accordance with earlier observations [17,20,21,71] that under the conditions of cathodic delamination the reduction of the PPy makes it cation-permselective, i.e. insertion of cations from the defect (here K^+) maintains the charge neutrality, not the release of the 3-Nisa counterions.

For PPy-BTA with PVB topcoat delamination profiles and corresponding electrode potentials in the defects obtained for different BTA concentrations during entrapment are shown in Fig. 9. All applied PPy coatings show for the intact coating a potential that is comparable to PPy without entrapped inhibitor. However, the potential at the delaminated interface is higher than in the defect. A similar observation was made also in prior works [20–22] and might indicate incomplete delamination and a not very high ionic conductivity in the partially reduced conductive polymer (the latter most likely partially due to partial over-oxidation during deposition, but most likely also due to partial degradation by oxygen reduction).

After the delamination experiment, the reduced PPy coating can easily be peeled off from the Zn substrate due to the significantly decreased adhesion between coating and metal. Compared with the PPy (3 mA/cm^2) coating without entrapped BTA, the BTA-containing coating shows a significant decrease of the delamination rate for the coating with PPy-BTA(0.1 M) (see Fig. 9 (d)). For the PPy-BTA(0.001 M) coating (see Fig. 9 (a)), there no passivation of the defect or the delaminated interface is observed. This indicates that this coating releases only a very limited amount of BTA. Fig. 9 (d) shows that for the coating with the higher BTA content with time the potential in the reduced/delaminated area increases gradually and finally reaches about 0 mV_{SHE}. Additionally, a strong anodic shift of the corrosion potential in

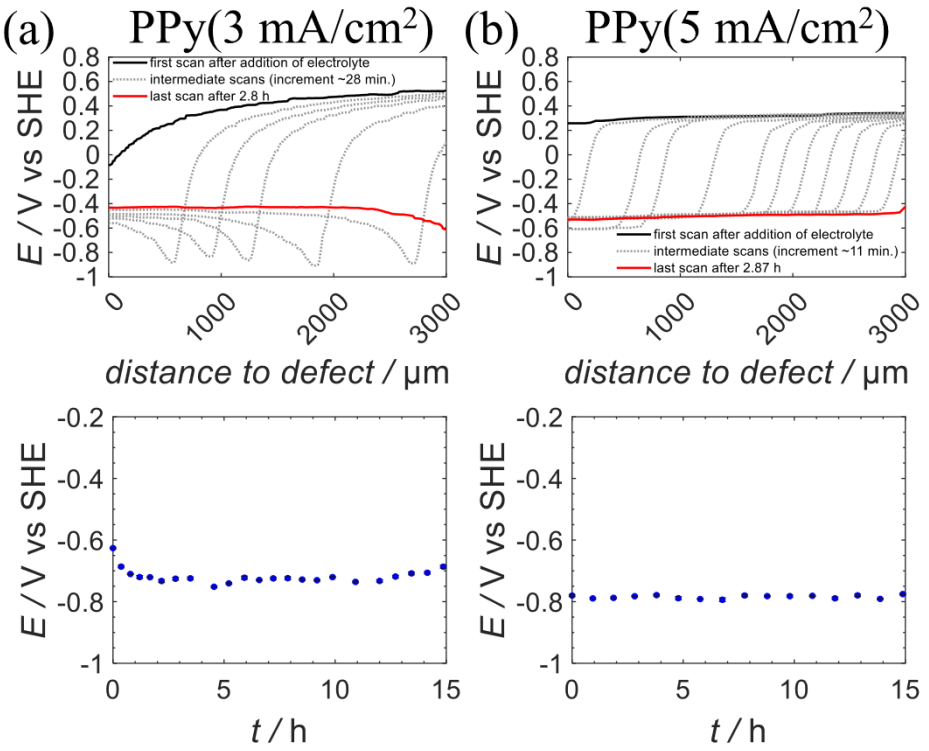

Fig. 8. Delamination profile for PPy electro-deposited onto pretreated zinc and the corresponding electrode potential at the defect site.

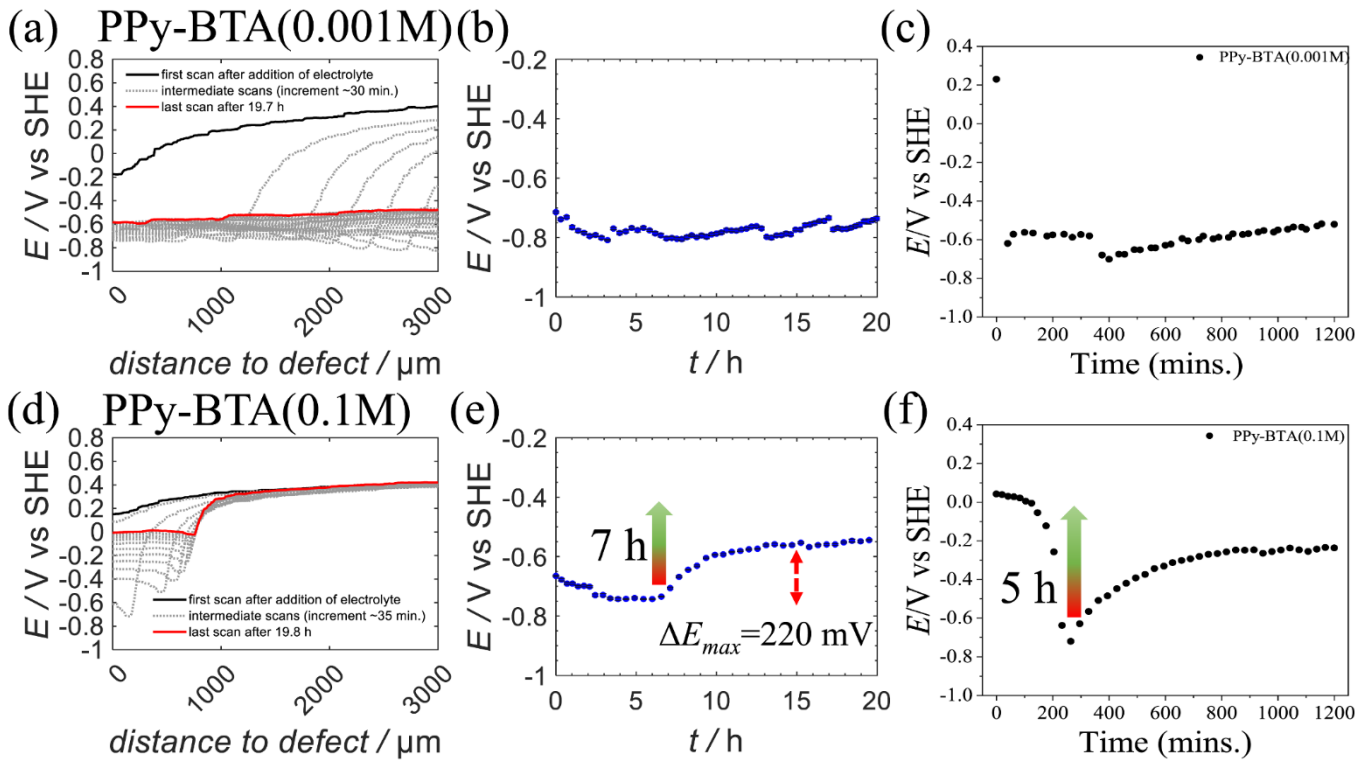

Fig. 9. SKP delamination profiles (a, d) and corrosion potential in the respective defects (b, e) monitored by SKP of PPy/PVB coatings on zinc with BTA corrosion inhibitor entrapped into PPy. (c, f) The potential evolution at the delaminating and delaminated interface at x = 500 μm from the (a) and (d).

the defect by 220 mV is observed for this coating with a high concentration of BTA in the PPy coating matrix. The increased potentials at the defect and the delaminated interface show that the released BTA can passivate the delaminated area and the defect site and then stop the corrosion of Zn substrate. The high potential re-established at the delaminated interface even indicates restoring of a blocking interface and partial re-oxidation of the PPy. This good performance is expected to be linked to a rapid release of BTA and its highly effective transport to the defect site.

In Fig. 9 (c, f) the potential at X = 500 μm is plotted as a function of

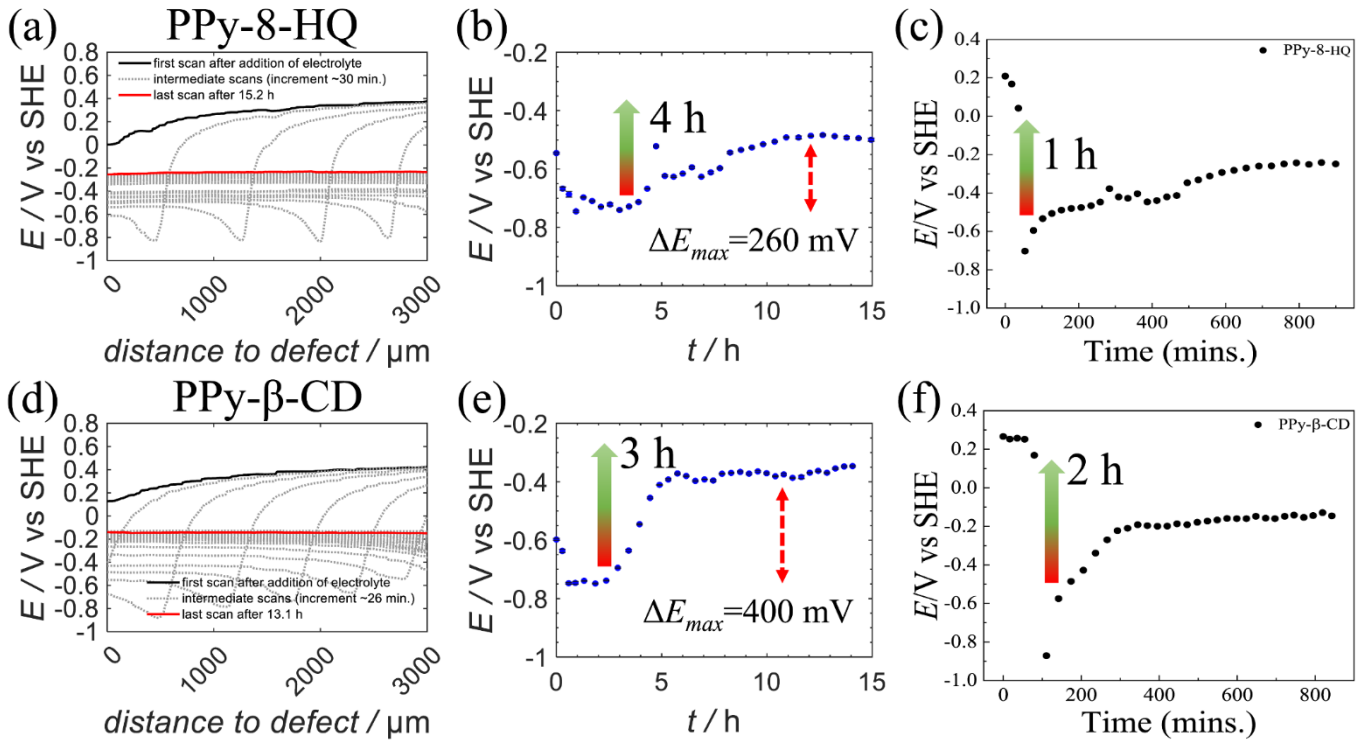

Fig. 10. SKP delamination profiles for (a, d) and electrode potential (b, e) of the PPy coating with corrosion inhibitor monitored by SKP. (c, f) The potential evolution at the delaminating and delaminated interface at x = 0.5 from (a, d).

the time, extracted from the data shown in Fig. 9 (a, d). In these plots the initial decrease of the potential is due to its delamination. From Fig. 9 (c), we can see that the potential at the delaminated area just stays low, indicating steady active corrosion of the zinc at the delaminated interface. However, for the PPy coating the higher concentration of entrapped BTA, the potential increases quite similar with the potential in the defect. After 5 h, the potential at the delaminated interface increases, while the one at the defect site needs 7 h to increase, i.e. the potential increase at the delaminated area advances the one in the defect which is most likely due to the faster supply of released BTA from the PPy coating.

Fig. 10 shows the cathodic delamination profiles and corrosion potentials in the defect for the same experiments carried now out with the PPy-8-HQ and PPy-β-CD coatings. The cathodic delamination profiles of these coatings, show a passivation of the defect and of the delaminated interface after only a few hours. For both the PPy-8-HQ and the PPy-β-CD coating, the initial delamination rates are a bit faster than the one of the PPy(5 mA/cm^2) coating in Fig. 8 (b). The presence of both inhibitors seems to accelerate the reduction rate of the PPy and that would mean the rate of cation incorporation. Thus, more coating is initially reduced and delaminated than for PPy-BTA in the same time. For both coatings passivation of the interface sets roughly in at the same time, but because of the initially faster delamination, more inhibitor is expected to be released for these two coatings before the delamination stops and a protective interface is restored and the PPy (partially) re-oxidized. In both cases the corrosion potential at the defect is observed to increase after about 5 h for PPy-8-HQ, by finally about 260 mV after 10 h, and for PPy-β-CD by about 400 mV, already after about 6 h. Fig. 10 (c, f) shows the development of the potential at the delaminating and delaminated interface at x = 0.5 mm (data from Fig. 10 (a, b)). As already for the case of PPy-BTA, it is also proposed here that this is due to the more ready availability of the released inhibitor at the interface compared to the defect. The quite high anodic shifts observed at the defect are proposed to be caused by a synergy between the effect of the inhibitor released into it and the oxidizing effect of the re-oxidized PPy, as it was already proposed in [21], where the transport of inhibitor through the partially reduced PPy was investigated and similar high anodic shifts were observed.

The above results prove that just entrapped corrosion inhibitor, i.e. in this case β-CD, 8-HQ and BTA, most likely all in the neutral state or positive charge, however, is released from the PPy network during reduction and that in sufficient amounts as to successfully passivate the defect and also the delaminated interface. This is different from counter-anions, which cannot be released due to the PPy becoming quickly cation permselective [71]. The observed good inhibition effect is proposed to be due to a synergetic action of PPy and corrosion inhibitor, as was shown already in our recent work [21].

Although the above observations are strong indications that the inhibitors are indeed entrapped into the PPy matrix, they show just indirectly that the release occurred as a consequence of PPy reduction. For providing a direct proof, also UV–vis spectroscopy was applied. First, spectra of BTA, tosylate and pyrrole monomer in 1 M KCl solution, separately and in combinations were measured (see Fig. 11). From the spectra, we can see that tosylate and pyrrole have a main peak located at 220 nm and 210 nm, respectively. For BTA there are two peaks at 208 nm and 257 nm. For tosylate and BTA in combination, there are clearly three peaks at 208 nm, 220 nm and 257 nm. For the combination of BTA, tosylate, pyrrole monomer the peak at 257 nm for BTA remains as a clear identifier for BTA. A strong peak at 212 nm results as a merger of the peaks at 208 nm, 210 nm and 220 nm from BTA, tosylate and pyrrole.

In order to obtain information about the release behavior of these PPy coatings two different kinds of release experiments were performed. One was performed by immersing the PPy coatings without topcoats into the electrolyte with and without low applied potential (of −500 mV_{SHE}, in order to reduce the PPy). This is denoted in the following as global release and leaching experiment and is what is more or less the standard

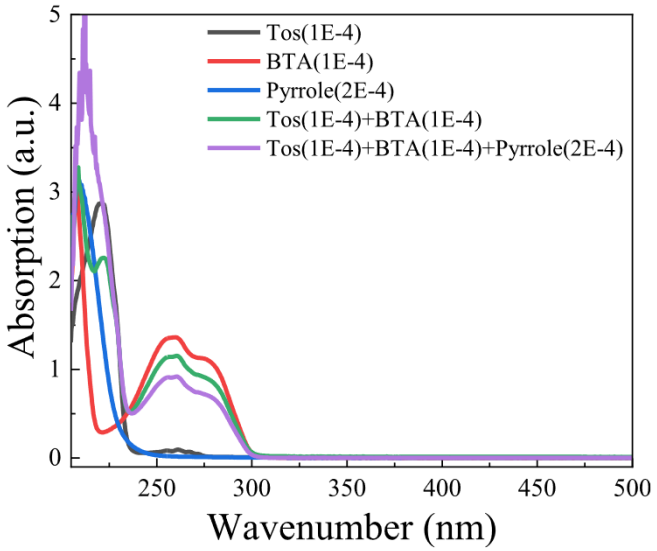

Fig. 11. The UV–vis spectra of purified BTA, tosylate and pyrrole in 1 M KCl solution before and after mixed each other.

experiment for inhibitor release from coatings in the literature. For this a layer of PPy(N(Et)$_4$Tos) coating was electrodeposited in the presence of 0.1 M BTA on an Au-coated Glass substrate. Gold was used here as an inert substrate, in order to have the focus solely on the coating. Furthermore, gold did not require to use 3-Nisa as counter-anion, which shows strong overlap with the BTA in UV–vis spectroscopy. Results obtained on leaching and release of entrapped BTA from this PPy(N(Et)$_4$Tos) coating in different electrolytes (1 M KCl and 0.05 M tetrabutylammonium chloride) are shown in Fig. 12. When the PPy coating is immersed in 1 M KCl solution, a broad peak at 257 nm reflects BTA leaching from the PPy(N(Et)$_4$Tos) coating (see Fig. 12 (a)). A strong peak at 220 nm represent the overlap of the BTA, tosylate and pyrrole monomer. Since in this experiment without applied potential the PPy is not reduced, the BTA release from coating is just dominated by diffusion inside the non-reduced PPy matrix. However, when the PPy is reduced, the situation is different (see Fig. 12 (b)). The peak at 200 nm is now stronger, i.e. more tosylate and pyrrole were released from the PPy coating. Also, the intensity of the BTA at 257 nm increased similarly. The increased release of the tosylate upon reduction of the PPy is expected, as for the case of mere immersion the counter-anions can only be released by exchange with chloride. Ingress of chloride and release of tosylate both have then to occur into or from the un-reduced PPy. For the case that the PPy is electrochemically reduced by the application of a low potential charge neutrality requires either release of the counter-anions or incorporation of cations.

Since in this global release experiment the counter-anion can leave the PPy across its thickness (only about several micrometers), no full cation-permselectivity occurs and at least a considerable part of the counter-anions contributes to establishing the charge neutrality, i.e. not all occurs by cation incorporation. For this reason, the release of tosylate is higher (and faster) for the case of reduction compared to mere immersion. In fact, it is quite remarkable that quite a significant part of the tosylate is released by mere immersion, i.e. by exchange with chloride. That also the release of the entrapped BTA is increased by reduction is proposed to be a result of structural changes in the PPy caused by the reduction. These are also assumed to be the reason for the release of higher amounts of pyrrole. When tetrabutylammonium chloride is used as electrolyte (see Fig. 12 (c)), the large cation cannot be incorporated into the PPy matrix upon reduction and hence the charge neutrality has to achieved solely by the release of tosylate. Hence, the release of tosylate is a bit higher for PPy reduction in this electrolyte. Interestingly, this is also the case for BTA, confirming the assumption that the release

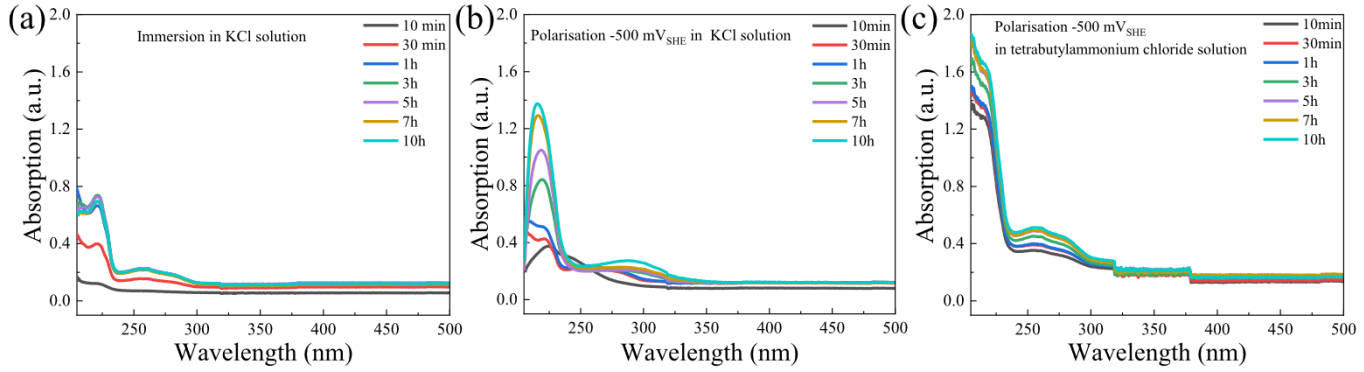

Fig. 12. (a) UV–vis spectra of PPy(N(Et)$_4$Tos)-BTA coating immersion in KCl. (b, c) apply −500 mV potential to reduction of PPy(N(Et)$_4$Tos)-BTA coating in the corresponding electrolyte.

of entrapped BTA is a consequence of structural changes induced by the PPy reduction. This means that the entrapped BTA is released as consequence of electrochemical reduction. Hence, also for entrapped inhibitor triggered release is possible.

In order to simulate the real release situation, another, second kind of release experiment was designed, which simulates the situation during delamination from defect for the case of atmospheric corrosion and/or a topcoat applied onto the PPy coating. This is denoted in the following as edge-release. Here, a layer of PPy(N(Et)$_4$Tos) coating was electrodeposited in the presence of 0.1 M BTA on an Au-coated glass substrate and then coated by a PVB topcoat. For this experiment, just the edge of the PPy coating was in contact with the electrolyte. Fig. 13 shows the release of BTA from the PPy coating into KCl solution with and without polarization for 10 h. Since the situation is different from the one during the global release, the intensities cannot be directly compared with the ones shown in Fig. 12 (a-c). However, what can be clearly seen from Fig. 13 is that there is a significant difference in leaching without applying a low potential and release upon applying one. Especially striking is the difference in intensity of BTA, which is significantly increased for the case of PPy reduction, while the tosylate peak (for the case with applied potential visible as shoulder in the first peak) seems unaltered. The similar intensity for tosylate in the two cases is proposed to be due to the PPy becoming quickly cation permselective in this setup, as here the transport has to occur in the lateral direction over much larger distances than for the case of global release. Hence, the reduction occurs mainly via cation incorporation. Hence, no enhanced release of counter-anions compared to the leaching without polarization occurs. However, BTA and also pyrrole (see the large peak around 220 nm and Fig. 11) show a significantly enhanced release upon reduction. That shows that for the release of BTA (and pyrrole) the change in PPy matrix structure due to its reduction suffices for increasing the release kinetics, i.e. the release of BTA is not affected by the cation permselectivity. This is because BTA is just entrapped and not incorporated as a counter-anion.

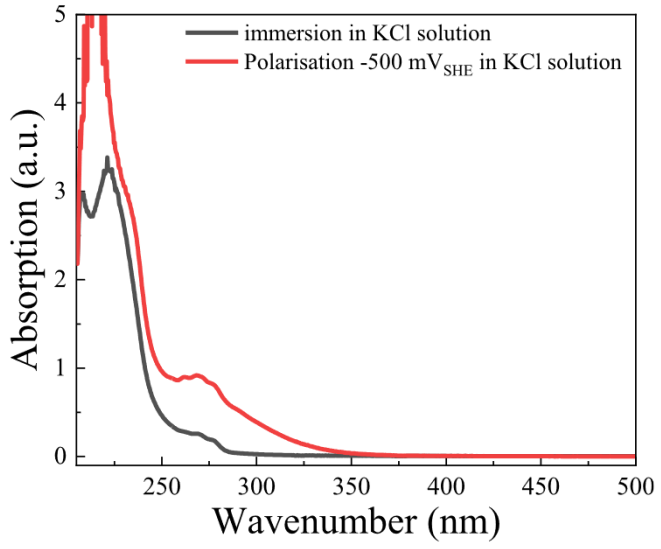

Fig. 13. UV–vis spectra of PPy(N(Et)$_4$Tos)-BTA coating immersion or polarization −500 mV$_{SHE}$ in KCl solution.

4. Conclusions

PPy coatings with entrapped neutral inhibitor molecules were successfully prepared on zinc from aqueous 3-Nisa solution containing pyrrole monomer and the neutral inhibitor molecules to be entrapped. While the 3-Nisa is incorporated as counter-anion to the positive charge at the polymeric backbone of the PPy, BTA, β-CD or 8-HQ are just entrapped as uncharged (or for BTA most likely initially positive) molecules within the polymer. It was shown that the PPy-BTA, PPy-β-CD and PPy-8-HQ coatings have the ability to passivate corroding defects inflicted into the coating through release of the corrosion inhibitor from the reduced PPy coating. While the 3-Nisa counter-anion is only released in small amounts, because the continuous PPy layer is turning cation-permselective upon reduction, the entrapped neutral inhibitor molecule is released in sufficient quantities as to passivate the defect and also the delaminated interface, which is even restored as a protective interface and the PPy is (partially) re-oxidized. This opens up a completely new strategy for intelligent release of active agents directly from ICP layers. It was shown that the potential triggered release of BTA, β-CD and 8-HQ entrapped into PPy causes an increase of the corrosion potential in the defect by more than 200 mV, for the β-CD even by about 400 mV. The proposed inhibition mechanism in the defect is a synergy between the effect of the inhibitor and anodic polarization by the re-oxidizing PPy. The latter is enabled by the onset of passivation of the metal at delaminated interface and restoration of a protective interface, which precedes the passivation of the defect.

CRediT authorship contribution statement

Yue Yin: Conceptualization, Investigation, Methodology, Validation, Writing – original draft, Writing – review & editing. **Manoj Prabhakar:** Methodology, Validation. **Petra Ebbinghaus:** Methodology, Validation. **Cauê Corrêa da Silva:** Methodology, Validation. **Michael Rohwerder:** Supervision, Validation, Writing – review & editing.

Declaration of Competing Interest

The authors declare that they have no known competing financial

interests or personal relationships that could have appeared to influence the work reported in this paper.

Acknowledgments

Yue Yin gratefully acknowledges the financial support from China Scholarship Council funding and Max-Planck Society for partially funding.

References

[1] B.R. Hou, X.G. Li, X.M. Ma, C.W. Du, D.W. Zhang, M. Zheng, W.C. Xu, D.Z. Lu, F. B. Ma, The cost of corrosion in China, npj Mater, Degrad. 1 (2017) 1–10.
[2] B. Hou (Ed.), The Cost of Corrosion in China, Springer Singapore, Singapore, 2019.
[3] O. Gharbi, S. Thomas, C. Smith, N. Birbilis, Chromate replacement: what does the future hold? npj Mater, Degrad. 2 (2018) 1–8.
[4] R.L. Twite, G.P. Bierwagen, Review of alternatives to chromate for corrosion protection of aluminum aerospace alloys, Prog. Org. Coat. 33 (2) (1998) 91–100.
[5] M.W. Kendig, R.G. Buchheit, Corrosion inhibition of aluminum and aluminum alloys by soluble chromates, chromate coatings, and chromate-free coatings, Corros. 59 (5) (2003) 379–400.
[6] D.E. Tallman, G. Spinks, A. Dominis, G.G. Wallace, Electroactive conducting polymers for corrosion control: Part 1. General introduction and a review of non-ferrous metals, J. Solid State Electrochem. 6 (2002) 73–84.
[7] N. Wint, A. Bennett, G. Williams, H.N. McMurray, The effect of phase continuity on the cathodic delamination resistance of polyaniline based coatings, J. Electrochem. Soc. 165 (13) (2018) C890–C899.
[8] P.P. Deshpande, N.G. Jadhav, V.J. Gelling, D. Sazou, Conducting polymers for corrosion protection: a review, J. Coat. Technol. Res. 11 (4) (2014) 473–494.
[9] M. Rohwerder, Conducting polymers for corrosion protection: a review, Int. J. Mater. Res. 100 (10) (2009) 1331–1342.
[10] F. Gao, J. Mu, Z. Bi, S. Wang, Z. Li, Recent advances of polyaniline composites in anticorrosive coatings: A review, Prog. Org. Coat. 151 (2021) 106071.
[11] S.A. Umoren, M.M. Solomon, Protective polymeric films for industrial substrates: A critical review on past and recent applications with conducting polymers and polymer composites/nanocomposites, Prog. Mater. Sci. 104 (2019) 380–450.
[12] D. Sazou, P.P. Deshpande, Conducting polyaniline nanocomposite-based paints for corrosion protection of steel, Chem. Pap. 71 (2) (2017) 459–487.
[13] P.J. Kinlen, D.C. Silverman, C.R. Jeffreys, Corrosion protection using polyanujne coating formulations, Synth. Met. 85 (1-3) (1997) 1327–1332.
[14] G. Paliwoda-Porebska, M. Stratmann, M. Rohwerder, K. Potje-Kamloth, Y. Lu, A. Z. Pich, H.-J. Adler, On the development of polypyrrole coatings with self-healing properties for iron corrosion protection, Corros. Sci. 47 (12) (2005) 3216–3233.
[15] A. Michalik, M. Rohwerder, Conducting polymers for corrosion protection: A critical view, Z. Phys. Chem. 219 (11) (2005) 1547–1559.
[16] P.J. Kinlen, V. Menon, Y. Ding, A mechanistic investigation of polyaniline corrosion protection using the scanning reference electrode technique, J. Electrochem. Soc. 146 (10) (1999) 3690–3695.
[17] M. Rohwerder, A. Michalik, Conducting polymers for corrosion protection: What makes the difference between failure and success? Electrochim. Acta 53 (2007) 1300–1313.
[18] D. Crespy, K. Landfester, J. Fickert, M. Rohwerder, Self-healing for anticorrosion based on encapsulated healing agents, Adv. Polym. Sci. 273 (2016) 219–246.
[19] U. Rammelt, L.M. Duc, W. Plieth, Improvement of protection performance of polypyrrole by dopant anions, J. Appl. Electrochem. 35 (12) (2005) 1225–1230.
[20] M. Uebel, L. Exbrayat, M. Rabe, T.H. Tran, D. Crespy, M. Rohwerder, On the role of trigger signal spreading velocity for efficient self-healing coatings for corrosion protection, J. Electrochem. Soc. 165 (16) (2018) C1017–C1027.
[21] Y. Yin, M. Schulz, M. Rohwerder, Optimizing smart self-healing coatings: Investigating the transport of active agents from the coating towards the defect, Corros. Sci. 190 (2021), 109661.
[22] A. Vimalanandan, L.-P. Lv, T.H. Tran, K. Landfester, D. Crespy, M. Rohwerder, Redox responsive self-healing for corrosion protection, Adv. Mater. 25 (48) (2013) 6980–6984.
[23] T.H. Tran, A. Vimalanandan, G. Genchev, J. Fickert, K. Landfester, D. Crespy, M. Rohwerder, Regenerative nano-hybrid coating tailored for autonomous corrosion protection, Adv. Mater. 27 (25) (2015) 3825–3830.
[24] X. Bai, T.H. Tran, D. Yu, A. Vimalanandan, X. Hu, M. Rohwerder, Novel conducting polymer based composite coatings for corrosion protection of zinc, Corros. Sci. 95 (2015) 110–116.
[25] M. Rui, Y.L. Jiang, A.P. Zhu, Sub-micron calcium carbonate as a template for the preparation of dendrite-like PANI/CNT nanocomposites and its corrosion protection properties, Chem. Eng. J. 385 (2020), 123396.
[26] P. Najmi, N. Keshmiri, M. Ramezanzadeh, B. Ramezanzadeh, Synthesis and application of Zn-doped polyaniline modified multi-walled carbon nanotubes as stimuli-responsive nanocarrier in the epoxy matrix for achieving excellent barrier-self-healing corrosion protection potency, Chem. Eng. J. 412 (2021), 128637.
[27] H.Y. Chen, H.Z. Fan, N. Su, R.Y. Hong, X.S. Lu, Highly hydrophobic polyaniline nanoparticles for anti-corrosion epoxy coatings, Chem. Eng. J. 420 (2021), 130540.
[28] F.Y. Li, Y.J. Ma, L. Chen, H.X. Li, H.D. Zhou, J.M. Chen, In-situ polymerization of polyurethane/aniline oligomer functionalized graphene oxide composite coatings with enhanced mechanical, tribological and corrosion protection properties, Chem. Eng. J. 425 (2021), 130006.
[29] D. Kowalski, M. Ueda, T. Ohtsuka, Corrosion protection of steel by bi-layered polypyrrole doped with molybdophosphate and naphthalenedisulfonate anions, Corros. Sci. 49 (3) (2007) 1635–1644.
[30] D. Kowalski, M. Ueda, T. Ohtsuka, Self-healing ion-permselective conducting polymer coating, J. Mater. Chem. 20 (2010) 7630–7633.
[31] H.K. Ryu, N. Sheng, T. Ohtsuka, S. Fujita, H. Kajiyama, Polypyrrole film on 55% Al-Zn-coated steel for corrosion prevention, Corros. Sci. 56 (2012) 67–77.
[32] D.M. Lenz, M. Delamar, C.A. Ferreira, Improvement of the anticorrosion properties of polypyrrole by zinc phosphate pigment incorporation, Prog. Org. Coat. 58 (1) (2007) 64–69.
[33] M. Sabouri, T. Shahrabi, H.R. Faridi, M.G. Hosseini, Polypyrrole and polypyrrole-tungstate electropolymerization coatings on carbon steel and evaluating their corrosion protection performance via electrochemical impedance spectroscopy, Prog. Org. Coat. 64 (4) (2009) 429–434.
[34] K.R.L. Castagno, D.S. Azambuja, V. Dalmoro, Polypyrrole electropolymerized on aluminum alloy 1100 doped with oxalate and tungstate anions, J. Appl. Electrochem. 39 (1) (2009) 93–100.
[35] M.G. Hosseini, M. Sabouri, T. Shahrabi, Corrosion protection of mild steel by polypyrrole phosphate composite coating, Prog. Org. Coat. 60 (3) (2007) 178–185.
[36] N. Sheng, Y. Lei, A. Hyonoo, M. Ueda, T. Ohtsuka, Improvement of polypyrrole films for corrosion protection of zinc-coated AZ91D alloy, Prog. Org. Coat. 77 (11) (2014) 1724–1734.
[37] H. Qian, D. Xu, C. Du, D. Zhang, X. Li, L. Huang, L. Deng, Y. Tu, J.M.C. Mol, H. A. Terryn, Dual-action smart coatings with a self-healing superhydrophobic surface and anti-corrosion properties, J. Mater. Chem. A 5 (5) (2017) 2355–2364.
[38] M.L. Zheludkevich, K.A. Yasakau, A.C. Bastos, O.V. Karavai, M.G.S. Ferreira, On the application of electrochemical impedance spectroscopy to study the self-healing properties of protective coatings, Electrochem. commun. 9 (10) (2007) 2622–2628.
[39] I.A. Kartsonakis, S.G. Stanciu, A.A. Matei, E.K. Karaxi, R. Hristu, A. Karantonis, C. A. Charitidis, Evaluation of the protective ability of typical corrosion inhibitors for magnesium alloys towards the Mg ZK30 variant, Corros. Sci. 100 (2015) 194–208.
[40] A. Altin, M. Krzywiecki, A. Sarfraz, C. Toparli, C. Laska, P. Kerger, A. Zeradjanin, K. J.J. Mayrhofer, M. Rohwerder, A. Erbe, Cyclodextrin inhibits zinc corrosion by destabilizing point defect formation in the oxide layer, Beilstein J. Nanotechnol. 9 (2018) 936–944.
[41] C.C. Harley, V. Annibaldi, T. Yu, C.B. Breslin, The selective electrochemical sensing of dopamine at a polypyrrole film doped with an anionic β-cyclodextrin, J. Electroanal. Chem. 855 (2019), 113614.
[42] M. Mrad, L. Dhouibi, M.F. Montemor, E. Triki, Effect of doping by corrosion inhibitors on the morphological properties and the performance against corrosion of polypyrrole electrodeposited on AA6061-T6, Prog. Org. Coat. 72 (3) (2011) 511–516.
[43] Y.H. Lei, N. Sheng, A. Hyono, M. Ueda, T. Ohtsuka, Effect of benzotriazole (BTA) addition on polypyrrole film formation on copper and its corrosion protection, Prog. Org. Coat. 77 (2) (2014) 339–346.
[44] S. Wan, C.H. Miao, R.M. Wang, Z.F. Zhang, Z.H. Dong, Enhanced corrosion resistance of copper by synergetic effects of silica and BTA co-doped in polypyrrole film, Prog. Org. Coat. 129 (2019) 187–198.
[45] A. Leng, H. Streckel, M. Stratmann, The delamination of polymeric coatings from steel. Part 1: Calibration of the Kelvin probe and basic delamination mechanism, Corros. Sci. 41 (1999) 547–578.
[46] A. Yassar, J. Roncali, F. Garnier, Conductivity and conjugation length in poly(3-methylthiophene) thin films, Macromolecules 22 (2) (1989) 804–809.
[47] H.M. Hung, D.K. Linh, N.T. Chinh, L.M. Duc, V.Q. Trung, Improvement of the corrosion protection of polypyrrole coating for CT3 mild steel with 10-camphor-sulfonic acid and molybdate as inhibitor dopants, Prog. Org. Coat. 131 (2019) 407–416.
[48] T. Osaka, T. Fukuda, K. Ouchi, T. Nakajima, Electropolymerization of electroinactive polypyrrole film for a nonlinear MIM switching device, Denki Kagaku 59 (1991) 1019–1025.
[49] J.Q. Xu, Y.Q. Zhang, D.Q. Zhang, Y.M. Tang, H. Cang, Electrosynthesis of PAni/PPy coatings doped by phosphotungstateon mild steel and their corrosion resistances, Prog. Org. Coat. 88 (2015) 84–91.
[50] V. Jothi, A.Y. Adesina, A.M. Kumar, M.M. Rahman, J.S.N. Ram, Enhancing the biodegradability and surface protective performance of AZ31 Mg alloy using polypyrrole/gelatin composite coatings with anodized Mg Surface, Surf. Coat. Technol. 381 (2020), 125139.
[51] Z.H. Chen, W.Z. Yang, B. Xu, Y.Y. Guo, Y. Chen, X.S. Yin, Y. Liu, Corrosion behaviors and physical properties of polypyrrole-molybdate coating electropolymerized on carbon steel, Prog. Org. Coat. 122 (2018) 159–169.
[52] B. Ramezanzadeh, E. Ghasemi, F. Askari, M. Mahdavian, Synthesis and characterization of a new generation of inhibitive pigment based on zinc acetate/benzotriazole: Solution phase and coating phase studies, Dyes Pigm. 122 (2015) 331–345.
[53] B. Gao, B. Tan, Y. Liu, C. Wang, Y. He, Y. Huang, A study of FTIR and XPS analysis of alkaline-based cleaning agent for removing Cu-BTA residue on Cu wafer, Surf. Interface Anal. 51 (5) (2019) 566–575.
[54] Y. Bao, Y. Yan, Y. Chen, J.Z. Ma, W.B. Zhang, C. Liu, Facile fabrication of BTA@ZnO microcapsules and their corrosion protective application in waterborne polyacrylate coatings, Prog. Org. Coat. 136 (2019), 105233.
[55] H. Gao, Q. Li, Y. Dai, F. Luo, H.X. Zhang, High efficiency corrosion inhibitor 8-hydroxyquinoline and its synergistic effect with sodium dodecylbenzenesulphonate on AZ91D magnesium alloy, Corros. Sci. 52 (5) (2010) 1603–1609.

[56] S.Y. Shen, Y. Zuo, X.H. Zhao, The effects of 8-hydroxyquinoline on corrosion performance of a Mg-rich coating on AZ91D magnesium alloy, Corros. Sci. 76 (2013) 275–283.
[57] A. Dehghani, G. Bahlakeh, B. Ramezanzadeh, Beta-cyclodextrin-zinc acetylacetonate (β-CD@ZnA) inclusion complex formation as a sustainable/smart nanocarrier of corrosion inhibitors for a water-based siliconized composite film: Integrated experimental analysis and fundamental computational electronic/atomic-scale simulation, Compos. B. Eng. 197 (2020), 108152.
[58] X.G. Wang, Z.G. Luo, Z.G. Xiao, Preparation, characterization, and thermal stability of β-cyclodextrin/soybean lecithin inclusion complex, Carbohydr. Polym. 101 (2014) 1027–1032.
[59] K.M. Cheung, D. Bloor, G.C. Stevens, Characterization of polypyrrole electropolymerized on different electrodes, Polymer 29 (1988) 1709–1717.
[60] L. Viau, J.Y. Hihn, S. Lakard, V. Moutarlier, V. Flaud, B. Lakard, Full characterization of polypyrrole thin films electrosynthesized in room temperature ionic liquids, water or acetonitrile, Electrochim. Acta 137 (2014) 298–310.
[61] N. Sheng, T. Ohtsuka, Preparation of conducting poly-pyrrole layer on zinc coated Mg alloy of AZ91D for corrosion protection, Prog. Org. Coat. 75 (1-2) (2012) 59–64.
[62] A. El Jaouhari, M. Laabd, E.A. Bazzaoui, A. Albourine, J.I. Martins, R. Wang, G. Nagy, M. Bazzaoui, Electrochemical and spectroscopical studies of polypyrrole synthesized on carbon steel from aqueous medium, Synth. Met. 209 (2015) 11–18.
[63] J. Molina, J. Fernández, A.I. del Río, J. Bonastre, F. Cases, Chemical, electrical and electrochemical characterization of hybrid organic/inorganic polypyrrole/$PW_{12}O_{40}^{3-}$ coating deposited on polyester fabrics, Appl. Surf. Sci. 257 (23) (2011) 10056–10064.
[64] J. Molina, J. Fernández, A.I. del Rio, J. Bonastre, F. Cases, Electrochemical synthesis of polyaniline on conducting fabrics of polyester covered with polypyrrole/$PW_{12}O_{40}^{3-}$. Chemical and electrochemical characterization, Synth. Met. 161 (2011) 953–963.
[65] W. Su, J.O. Iroh, Surface composition and topography of electrodeposited polypyrrole coatings on steel substrates, J. Adhes. 73 (2-3) (2000) 215–231.
[66] J. Molina, F.R. Oliveira, A.P. Souto, M.F. Esteves, J. Bonastre, F. Cases, Enhanced adhesion of polypyrrole/$PW_{12}O_{40}^{3-}$ hybrid coatings on polyester fabrics, J. Appl. Polym. Sci. 129 (2013) 422–433.
[67] C.A.J. Richards, H.N. McMurray, G. Williams, Smart-release inhibition of corrosion driven organic coating failure on zinc by cationic benzotriazole based pigments, Corros. Sci. 154 (2019) 101–110.
[68] T.F. Liu, W. Li, C.Y. Zhang, W. Wang, W.W. Dou, S.G. Chen, Preparation of highly efficient self-healing anticorrosion epoxy coating by integration of benzotriazole corrosion inhibitor loaded 2D-COF, J. Ind. Eng. Chem. 97 (2021) 560–573.
[69] E. Gaidamauskas, E. Norkus, E. Butkus, D.C. Crans, G. Grincienė, Deprotonation of β-cyclodextrin in alkaline solutions, Carbohydr. Res. 344 (2) (2009) 250–254.
[70] S.Y. Park, P. Ghosh, S.O. Park, Y.M. Lee, S.K. Kwak, O.H. Kwon, Origin of ultraweak fluorescence of 8-hydroxyquinoline in water: photoinduced ultrafast proton transfer, RSC Adv. 6 (2016) 9812–9821.
[71] G. Paliwoda-Porebska, M. Rohwerder, M. Stratmann, U. Rammelt, L.M. Duc, W. Plieth, Release mechanism of electrodeposited polypyrrole doped with corrosion inhibitor anions, J. Solid State Electrochem. 10 (9) (2006) 730–736.